Colloids and Surfaces A: Physicochemical and Engineering Aspects 682 (2024) 132900

Contents lists available at ScienceDirect

Colloids and Surfaces A: Physicochemical and Engineering Aspects

journal homepage: www.elsevier.com/locate/colsurfa

Rapid preparation of porous carbon by Flash Joule heating from bituminous coal and its adsorption mechanism of methylene blue

Qiang Li [a], Yajun Wang [a], Rongtao Zhu [a,b], Junchen Wu [a], Wenjun Zhang [a,b,*], Haozhi Lu [a]

[a] School of Chemical Engineering and Technology, China University of Mining and Technology, Xuzhou 221116, Jiangsu, China
[b] Key Laboratory of Coal Processing and Efficient Utilization of Ministry of Education, China University of Mining and Technology, Xuzhou 221116, Jiangsu, China

GRAPHICAL ABSTRACT

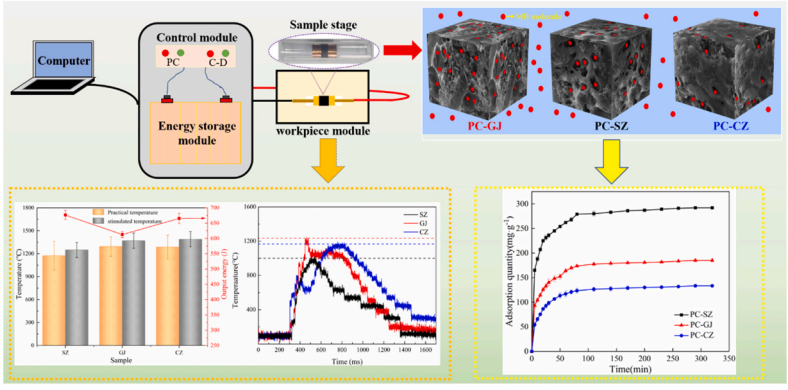

ARTICLE INFO

Keywords:
Porous carbon
Flash Joule heating
Bituminous coal with different degrees of metamorphism
Adsorption mechanism

ABSTRACT

Porous carbon is an extensively used adsorbent for the removal of dye. However, the conventional high-temperature carbonization and activation method with prolonged heating and annealing process was complicated, energy-consuming and polluting, which greatly limit the large-scale production. In this study, rapid and efficient preparation of porous carbon by the Flash Joule heating (FJH) method was realized for the first time using three bituminous coal samples with different degrees of metamorphism. The preparation process was completed in less than 1 s without chemical treatment, the process was more environmentally friendly. The physical and chemical properties of porous carbon were analyzed and the adsorption mechanism of porous carbon on methylene blue (MB) was investigated. The results showed that the specific surface area of porous carbon prepared by Shuozhou (PC-SZ), Gujiao (PC-GJ) and Changzhi (PC-CZ) could reach 601.95, 361.91 and 256.33 $m^2 \cdot g^{-1}$, respectively. The diversity in chemical properties of coal with different metamorphic degrees leads to the different properties of porous carbon. PC-SZ had a higher content of oxygen-containing functional groups and defects. The adsorption experiments indicate that PC-SZ had the best adsorption capacity on MB. The adsorption process was fitted by pseudo-second-order model commendably. It was found that more lattice defects and larger interlayer spacing made PC-SZ to become an excellent adsorbent of methylene blue (MB). Therefore,

* Corresponding author at: School of Chemical Engineering and Technology, China University of Mining and Technology, Xuzhou 221116, Jiangsu, China.
E-mail address: zwjcumt@cumt.edu.cn (W. Zhang).

https://doi.org/10.1016/j.colsurfa.2023.132900
Received 27 September 2023; Received in revised form 27 November 2023; Accepted 29 November 2023
Available online 1 December 2023

FJH can be an innovative approach for preparing porous carbon with excellent adsorption properties and is expected to achieve large-scale production.

1. Introduction

Coal is an inexpensive carbon source with a unique carbon structure and abundant mineral composition. Converting it into carbon material has unique advantages and prospects, which is of great significance to implementing efficient conversion and utilization of coal resources [1]. The performance of coal-based porous carbon was severely limited by the preparation method. Presently, the preparation of porous carbon mainly includes carbonization and activation processes [2]. The carbonization process is inevitable. There are one-step [3] and multi-stage [4] activation methods that require complex processes. The traditional furnace heating method is mostly used for low-temperature carbonization and high temperature activation [5–7]. These methods are time-consuming, labor-intensive and energy-intensive, which limit the large-scale production of porous carbon. At present, researchers mainly prepare porous carbon with the required performance by selecting different materials and special treatment methods. Zhang et al. utilized microwave technology to prepare porous carbon with specific surface area of 2768.52 $m^2 \cdot g^{-1}$ from chili straw pyrolysis residue [8]. Liu et al. used potassium cinnamate as raw material to prepare honeycomb porous carbon with a specific surface area of 2198 $m^2 \cdot g^{-1}$ [9]. Tian et al. reported that porous carbon made of low-rank coal and oxidized pellets had well-developed mesopores with a specific surface area of 370.42 $m^2 \cdot g^{-1}$ [10]. However, these categories required high temperature equipment and were time-consuming. Flash Joule heating (FJH) is a typical non-radiative heating method, which utilizes the electrical resistance exotherm of the sample to generate instantaneous high temperature within 1 s allowing a rapid conversion of the coal sample with lower energy consumption [11]. It could convert carbon sources into graphene [12–16]. Carbonization and pore formation of materials can also be achieved at low temperatures (below 1500 K). At present, there has been extensive research on the preparation of graphene by FJH. However, the research concerning the microstructure evolution of coal-based porous carbon prepared from different metamorphic degree bituminous coal by the FJH method is not well understood.

Coal-based porous carbon with excellent electrochemical performance has been widely used for supercapacitor [17], battery material [18], and catalytic material [19]. Besides, the high specific surface area of coal-based porous carbon makes it possible to be used as an efficient adsorbent. For instance, coal-based porous carbon has extensive applications in gas adsorption or storage, wastewater treatment, and other fields. Moreover, the controllable pore structure of porous carbon is a prerequisite for high-quality adsorption material. Wang et al. regulated the inherent minerals in coal precursor to produce high porosity coal-based porous carbon [20]. Vassileva et al. discussed the removal of ammonium ions and toxic ion from water using coal-based porous carbon [21,22]. Yi et al. studied the adsorption of lead(II) from aqueous solutions through porous carbon, and the adsorption quantity reached 162.33 $mg \cdot g^{-1}$ [23]. To summarize, coal-based porous carbon can achieve effective elimination of organic and inorganic contaminants in water. However, the adsorption mechanism of coal-based porous carbon prepared by FJH on methylene blue (MB) dye wastewater is still unclear.

As a result, this study is dedicated to investigate the influence of bituminous coal metamorphism degree on the microstructure of Flash coal-based porous carbon and its adsorption mechanism. Porous carbons were prepared from bituminous coal with different degrees of metamorphism using FJH method. The pore structure and size distribution of porous carbon were analyzed. The physical and chemical properties of porous carbon were explored using various chemical analysis equipment. The adsorption performance of Flash coal-based porous carbon for MB was studied and the adsorption mechanism was determined. This study is expected to lay the foundation for developing new methods for coal-based carbon material preparation and elucidate the adsorption mechanism of MB on Flash coal-based porous carbon.

2. Materials and methodology

2.1. Materials

Three coal samples with different metamorphism degrees were obtained from Shuozhou (SZ), Gujiao (GJ) and Changzhi (CZ) of Shanxi Province, China. The degree of metamorphism in descending order was SZ, GJ and CZ. The coal samples were dried at 70 ℃ and then ground to less than 200 mesh. Float and sink test of three coal samples was conducted using heavy liquids with densities of 1.35, 1.41 and 1.42 $g \cdot cm^{-3}$ respectively to prepare ultra-low ash sample. The prepared coal samples and K_2CO_3 with a mass ratio of 1:3 were mixed in a reactor filled with deionized water and then dried using a heating oven for 6 h. Finally, it was vacuum dried for 10 h for subsequent FJH test. Table 1 listed the proximate analysis of raw coal and the prepared ultra-low ash coal samples. After deashing treatment, the ash content of three coal was reduced to around 3% and the fixed carbon content increased by more than 7%. The volatile content was slightly reduced.

The heavy liquid used in the experiment was composed of benzene, carbon tetrachloride and tribromomethane, all of which were produced by Tianjin Yifang Technology Co., Ltd. Potassium carbonate was produced by Xilong Chemical Co., Ltd. MB solution was purchase from Tianjin Ruijinte Chemical Co., Ltd. These purchased reagents used in the experiments were analytical pure. The deionized water was used in the experimental process.

2.2. Flash Joule heating experiment

The schematic diagram for FJH experiment of preparing coal-based porous carbon was shown in Fig. 1. The system was consist of control module, workpiece module, energy storage module, sample stage and computer[24]. The sample stage is made of a quartz tube with a length of 50 mm and a diameter of 8 mm. The prepared ultra-low ash coal samples were mixed with carbon black and activator (K_2CO_3) evenly in a ratio of 1:1:3 by mass to increase the conductivity of the samples. Firstly, a piece of graphite electrode was plugged into one end of the quartz tube, then 300 mg of powder sample was added to the quartz tube, and finally another piece of graphite electrode was plugged from the other end and the sample was compacted. To increase the tightness of graphite electrodes, a layer of copper foil was wrapped on the surface. Copper foil only served as a sealing material but not essential for experiments. Then the quartz tube was placed on the Flash Joule heating equipment. The sample was heated instantaneously at a flash voltage of 80 V and reacted with the activator through capacitance discharge. Flash coal-based porous carbon obtained by FJH of the three coal samples was recorded as PC-SZ, PC-GJ and PC-CZ, respectively.

Table 1
Proximate analysis of raw coal and ultra-low ash coal samples.

Coal samples	M_{ad}	A_{ad}	V_{daf}	FC_d
Shuozhou(raw)	2.30	14.24	38.72	51.15
Gujiao(raw)	0.70	11.76	20.69	69.43
Changzhi(raw)	0.66	12.00	13.30	74.60
Shuozhou(ultra-low ash)	2.50	3.03	37.92	58.65
Gujiao(ultra-low ash)	1.20	2.98	20.03	76.63
Changzhi(ultra-low ash)	0.90	3.05	12.88	83.68

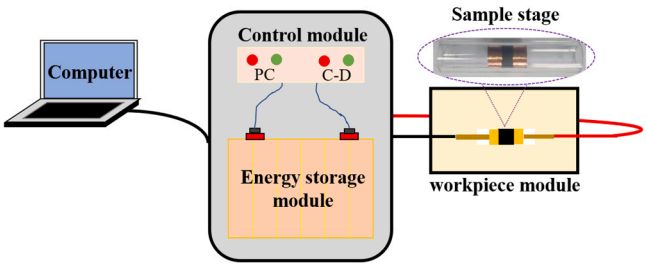

Fig. 1. Schematic diagram of the flash Joule heating device.

2.3. Flash Joule heating process simulation

The inner diameter of the quartz tube used in the simulation process was 6 mm, in which the sample was tightly compacted in the tube with a length of 5 mm. Both sides of the sample were two graphite electrodes with a thickness of 8 mm. The initial temperature of the sample was 293.15 K. The simulation process was carried out using COMSOL software. The parameters selected for the simulation process were shown in Table 2.

2.4. Structure analysis of Flash coal-based porous carbon

The microstructure of prepared Flash coal-based porous carbon was obtained by FE-SEM (Hitachi S-4800, Japan) with magnification from 0.5 to 50 kV. Before testing, the samples were glued to the sample holder with conductive adhesive and sprayed with gold. The adsorption isotherm of Flash coal-based porous carbon samples was measured at 77 K using a Micrometric ASAP2420 automatic adsorption instrument. The total specific surface area was calculated by the Brunner-Emmett-Teller (BET), the t-plot and the Barrett-Joyner-Halenda (BJH) method, respectively [25–27]. The total pore volume was determined using the nitrogen adsorption amount under a relative pressure of 0.99. The density functional theory was employed to obtain pore size distribution. Before testing, the moisture and gaseous impurities were removed by degassing at 180 ℃ for 8 h.

Flash coal-based porous carbon prepared from coal with different metamorphic degrees was ground to below 74 μm for analysis. A Raman spectrometer (HORIBA HR, Germany) was utilized to test the microcrystalline structure of all samples with a spectral resolution of $\leq 1.5\ cm^{-1}$ and a 532 nm excitation wavelength. The crystal structure of porous carbon was measured by X-ray diffraction analyzer (D8 Advan, Germany). The surface speciation analysis of these samples was conducted via X-ray photoelectron spectrometer (Nexsa, China) with the excitation source being A1Kα (1486.6 eV) X-ray. The oxygen content in coal and porous carbon was characterized by the O mode of organic element analyzer (Thermo FLASH 2000, America).

2.5. Methylene blue adsorption experiment

The MB adsorption experiment was conducted in a conical flask. The input dosage of Flash coal-based porous carbon was 50 mg. PC-SZ, PC-GJ, and PC-CZ were added to 200 mL prepared 100 $mg{\cdot}L^{-1}$ MB solution. Each experiment oscillated on a constant temperature water bath oscillator at a frequency of 200 $r{\cdot}min^{-1}$ at 25 ℃. After the adsorption process, 5 mL of liquids were sucked by pipette and then loaded into a centrifuge tube, followed by centrifugation using centrifuge (AXTG20G, China) with speed of 5000 $r{\cdot}min^{-1}$ for 5 min to obtain the supernatants. They were diluted to a certain concentration to ensure that absorbance was within the range of Beer's law. Ultraviolet spectrophotometer (Evolution 350, China) was employed at the wavelength of 664 nm to test the absorbance of the diluted supernatant and calculate the remaining concentration of MB solution [28,29].

Table 2
Parameters of COMSOL simulation.

Coal samples	σ/ S·m	ε_r	C_p/ J/ (kg·K)	k/ W/ (m·K)	ρ/ $kg{\cdot}m^{-3}$
Shuozhou	235	1	150	710	1400
Gujiao	310	1	150	710	1450
Changzhi	185	1	150	710	1470

The evaluation of the adsorption capacity of Flash coal-based porous carbon for MB was based on the removal rate of MB, which was obtained by Eq. (1). The amount of MB adsorbed on Flash coal-based porous carbon was calculated using Eq. (2).

$$R = \frac{C_0 - C_t}{C_0} \times 100\% \tag{1}$$

$$\Gamma = \frac{(C_0 - C_t + C_b) \times V}{m} \tag{2}$$

where R is removal rate of MB, %; C_0 is initial concentration of MB solution, $mg{\cdot}L^{-1}$; C_t is remained MB concentration in the solution after adsorption, $mg{\cdot}L^{-1}$; Γ represents the amount of MB adsorbed per unit mass of coal-based activated carbon, $mg{\cdot}g^{-1}$; C_b represents the concentration of blank sample after absorbance conversion, $mg{\cdot}L^{-1}$; V is the volume of MB solution with a value of 0.2 in this study, L; and m is the mass of coal-based porous carbon, g.

3. Results and discussion

3.1. Analysis of Flash Joule heating process

In order to prepare porous carbon with a high specific surface area, the selected Flash voltage was 80 V, which could avoid excessive graphitization of the sample. Because the high temperature was generated under high voltage.[24] The maximum temperature and output energy during the practical FJH process were shown in Fig. 2(a). It showed that the maximum temperature reached during the FJH process of PC-GJ was 1290 ℃ and the output energy was 613 J. The maximum temperature that can be reached during the PC-SZ preparation process was 1175 ℃ while the output energy was 677 J. Under the same conditions, the total energy remains unchanged, and the more energy used for temperature rise, the less remaining output energy. Fig. 2(b) illustrated the Flash temperature versus time during the practical FJH process, it showed that the reaction process of PC-SZ could be completed within 250 ms and the cooling time was only 900 ms. The reaction time of PC-GJ and PC-CZ was around 500 ms. It means that the process of preparing porous carbon by FJH can be completed in an instant without long heat treatment process.

Finite element simulation of the FJH process was processed using COMSOL software to analyze temperature fluctuations within the reaction zone of the sample. The simulated temperature changes during the preparation process of porous carbon were shown in Fig. 2(c-e). The comparison of the maximum temperature reached during the practical and simulation process was shown in Fig. 2(a). The maximum temperature of simulated was about 100 ℃ higher than that of practical due to the inhomogeneous of the actual samples and the energy loss in the FJH process. The temperature variation trends of the three types of porous carbon preparation processes were similar, but the time to reach the highest temperature was different. For SZ and GJ with low degree of metamorphism, the time to reach the highest temperature was relatively short. The temperature in the sample area was the highest, and the temperature gradually decreased as it extends to both sides vertically. It should be noted that the temperature of the graphite electrode is significantly lower than that of the sample, which indicated that the electrode would not cause excessive energy loss. The temperature was basically the same on the same horizontal plane. The heating of the sample was uniform. The increase in the degree of coal metamorphism may slightly increase the reaction time, possibly due to the stable structure of high metamorphic coal making the pore forming process

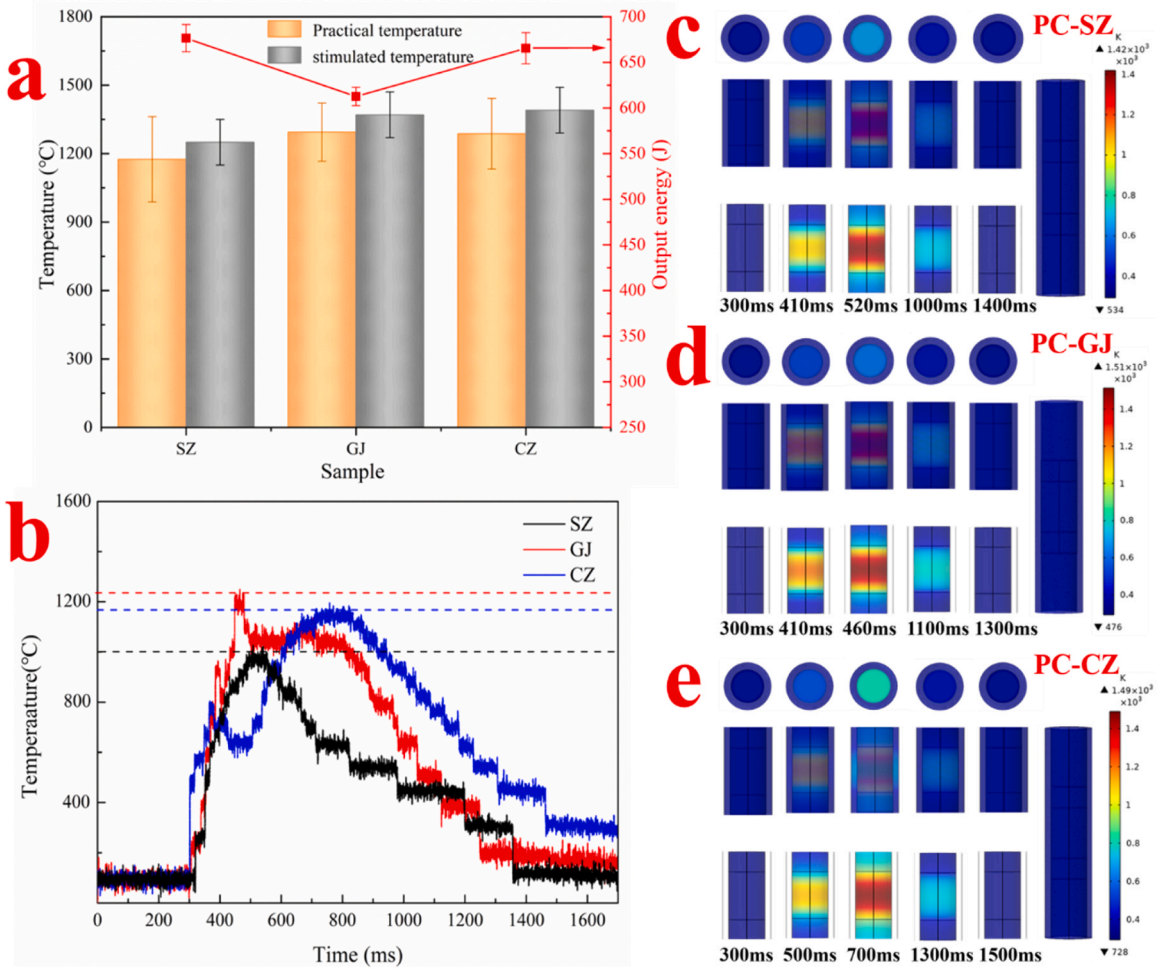

Fig. 2. (a) Maximum temperature and output energy during the practical and simulate FJH process; (b) Curve of Flash temperature versus time; (c-e) temperature clouds for the preparation process of PC-SZ, PC-GJ and PC-CZ by FJH using COMSOL simulation.

more difficult. The temperature trends obtained from simulation and practical of the porous carbon preparation process were in concurrence, thus evidencing the viability of the process.

The FJH method could instantly convert electrical energy into the heat required for sample reaction. Thereby, FJH process achieved rapid high-temperature preparation of porous carbon with low energy consumption. The heating and annealing times were short, greatly shortening the preparation process and time of porous carbon. Compared to traditional porous carbon production methods, it can significantly improve production efficiency and save reaction time. In addition, it has been shown that the FJH method reduced costs and pollutant gas emissions by more than 50% compared to methods such as synthetic graphite and hydrometallurgy.[30,31] The advantage of the FJH method is also highlighted by the high energy efficiency resulting from Joule's law.[32].

3.2. *Pore structure and size distribution of Flash coal-based porous carbon*

The pore structure, specific surface area and pore size distribution were closely related to the performance of Flash coal-based porous carbon. Firstly, the surface morphology of Flash coal-based porous carbon was obtained by SEM. Fig. 3 showed the SEM images of PC-SZ, PC-GJ and PC-CZ. It can be observed that the surface of PC-SZ was the roughest and developed a great quantity of cellular pores. The number of pores of PC-GJ decreased and the pore size increased. The surface of PC-

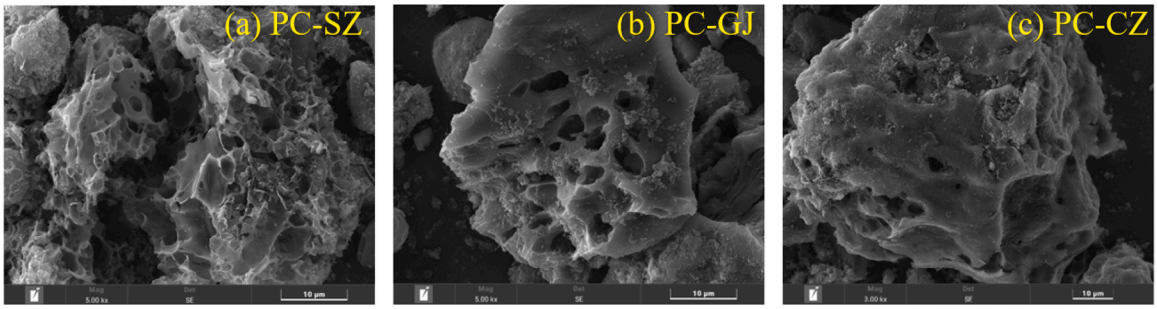

Fig. 3. SEM pictures of three Flash coal-based porous carbon.

CZ was the smoothest with fewer pores, possessing "Silk-Like" morphological characteristics. This may be due to the increased degree of coal metamorphism, making the carbon structure more stable and less prone to pore structure formation during the flash process. The Flash coal-based porous carbon tends to generate larger pores in the form of convolutions, which attributed to the destruction of the coal structure under the vigorous reaction conditions.

The N_2 adsorption method is a common method for analyzing the specific surface area of porous carbon. The N_2 adsorption isotherms of three raw coal and its Flash coal-based porous carbon were displayed in Fig. 4. PC-SZ adsorbed the highest amount of N_2 to reach the saturation state, followed by PC-GJ and PC-CZ. The adsorption quantity of raw coal was extremely low. The N_2 adsorption capacity of porous carbon decreased as the degree of metamorphism of raw coal increased. The more N_2 adsorption quantity indicated a higher specific surface area. It showed that the adsorption isotherms of porous carbon were well-modeled by typical I and IV Langmuir isotherm types, indicating the predominant presence of micropores. A hysteresis loop was observed clearly under a relative pressure of 0.5, which illustrated that the prepared porous carbon had a certain proportion of mesopores. The specific surface area and pore volume of three raw coal and its Flash coal-based porous carbon was listed in Table 3. The specific surface area of three raw coal was less than 2 $m^2 \cdot g^{-1}$. PC-SZ had the largest specific surface area of 601.95 $m^2 \cdot g^{-1}$. The specific surface area of PC-GJ and PC-CZ were 361.91 and 256.33 $m^2 \cdot g^{-1}$, respectively. The data agreed well with the N_2 adsorption results.

The high specific surface area of PC-SZ was related to the higher volatile matter. The release of gases during the FJH process promoted the formation of pores. Table 4 listed the preparation process and specific surface area of several coal based porous carbons reported in literatures. Obviously, the preparation of porous carbon inevitably required high-temperature carbonization and activation, which was energy-intensive and time-consuming. Inert gas protection was required during the heating process, which increased the preparation cost. However, FJH method does not require these complex processes and could achieve the preparation of porous carbon within 1 s. The porous carbon prepared simultaneously has a considerable specific surface area. It indicated that FJH could facilitate the preparation of porous carbon with high specific surface area.

In addition to specific surface area, pore size distribution also affected the performance of porous carbon. Fig. 5 showed the pore size distribution of three Flash coal-based porous carbon. According to the standards of International Union of Pure and Applied Chemistry (IUPAC), pores were divided the pores into micropores (<2 nm), mesopores (2–50 nm) and macropores (>50 nm) [39]. Fig. 5 showed that the proportion of micropores in three types porous carbon occupied advantage and most of the pores were less than 1 nm. The number of mesopores and macropores was relatively fewer. The content of macropores was almost consistent among the three types of porous carbon. The number of pores was associated with the activator and volatile matter. The higher the volatile content, the more pores would be formed after escaping at high temperature, which was conducive to the activator entering the internal of coal to form enrichment pore structure.

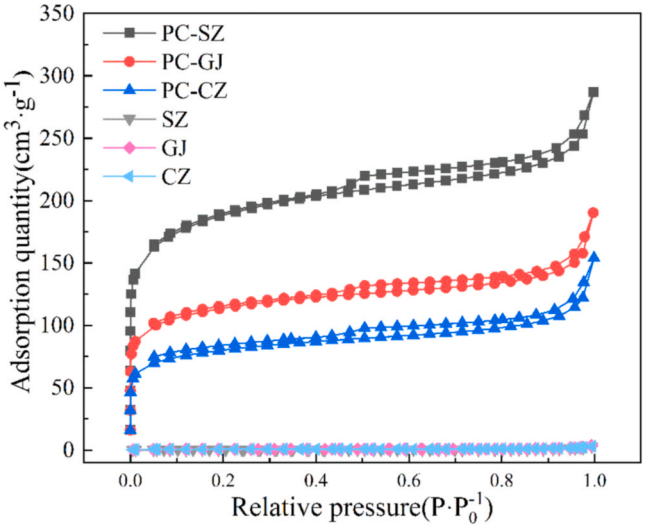

Fig. 4. N_2 adsorption isotherm of three Flash coal-based porous carbon.

Table 3
The specific surface area and total pore volume of three Flash coal-based porous carbon.

Samples	Specific surface area/ $m^2 \cdot g^{-1}$	Specific surface area of micropores/ $m^2 \cdot g^{-1}$	Total pore volume/ $cm^3 \cdot g^{-1}$	Micropore volume/ $cm^3 \cdot g^{-1}$
SZ	0.66	0.56	-	-
GJ	1.63	0.66	-	-
CZ	1.87	0.51	-	-
PC-SZ	601.95	328.98	0.44	0.17
PC-GJ	361.91	207.53	0.29	0.11
PC-CZ	256.33	142.53	0.24	0.07

Table 4
Preparation process and specific surface area of coal-based porous carbon.

Materials and ash removal method	activator	Preparation process	Specific surface area/ $m^2 \cdot g^{-1}$	Ref.
anthracite; HCl and HF washing	NaOH	activated by H_2SO_4 in an ice-water bath condition, $KMnO_4$ oxidation and freeze-drying for 12 h, Tube furnace, 700 ℃ under nitrogen atmosphere	402.00	[18]
sub-bituminous coal; HCl and HF washing	mineral-Loaded	Tube furnace, 900 ℃ under nitrogen & carbon dioxide atmosphere for 1 h, acid wash to neutral	933.00	[20]
Lignite; HCl and HF washing	$ZnCl_2$	Tube furnace, 550 ℃ under nitrogen atmosphere for 1.5 h, acid wash to neutral	731.48	[33]
Bituminous coal; HCl washing	Steam	Tube furnace, 800 ℃ under nitrogen & steam atmosphere for 3 h	338.30	[34]
Dahuangshan coal; H_2SO_4 and H_2NO_3 washing	Air, Steam	Electrospinning & Tube furnace, 280 ℃ for 3 h in Air, 800 ℃ for 1 h in Ar, 800 ℃ for 30 min with steam	902.00	[35]
Zhundong coal	CO_2 and H_2O co-activation	Tube furnace, 800 ℃ under nitrogen atmosphere for 2 h to carbonize activate	556.21	[36]
Coal	KOH	Tube furnace, 800 ℃ under nitrogen atmosphere for 2 h, water washing	1225.38	[37]
coal pitch; modified by chemical cross-linking	KOH	Tube furnace, charred at 500 ℃ under nitrogen atmosphere for 40 min, activation at 600 ℃ under nitrogen atmosphere for 2 h	around 650.00	[38]
bituminous coal; Float and sink experiment	K_2CO_3	Flash Joule heating method, reaction process is completed within 1 s without chemical treatment	602.95, 362.91, 256.33	This work

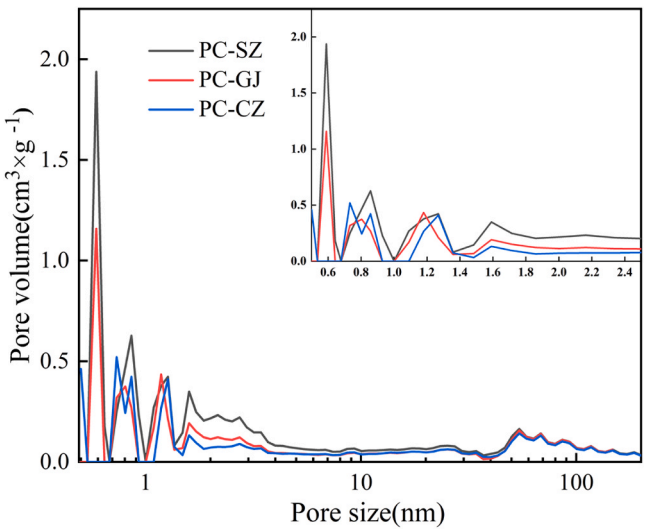

Fig. 5. Pore size distribution of three Flash coal-based porous carbon.

Instantaneous high-voltage discharge caused a large number of volatile components to escape, resulting in "thermal expansion effect". Meanwhile, a huge number of pores will remain in the coal. However, the escaping gases cannot be released in a timely manner, which led to an increase in pressure inside the quartz tube and made it easier for the activator to enter the pore channels etching the coal sample. It led to the rich pore structure of PC-SZ.

3.3. Structure of Flash coal-based porous carbon

Crystal structure is an important property of porous carbon. The crystal structure of Flash coal-based porous carbon was examined by XRD. Fig. 6(a) showed the XRD spectra of three types of Flash coal-based porous carbon. It can be seen that three types of porous carbon had apparent (002) characteristic peak with larger half peak widths, proving the stacking layer structure in porous carbon. The ordered degree of layered structure in porous carbon was relatively low. The peak position of (002) was around 24.8°. The interlayer spacing of porous carbon was calculated using the Bragg equation: $2d\sin\theta=n\lambda$. The result was about 0.36 nm. Weak (100) characteristic peak appeared around 43°. The (002) peak significantly increased and the peak position gradually shifted towards a higher angle with the increase of raw coal metamorphism degree. It indicated that the layers of porous carbon were

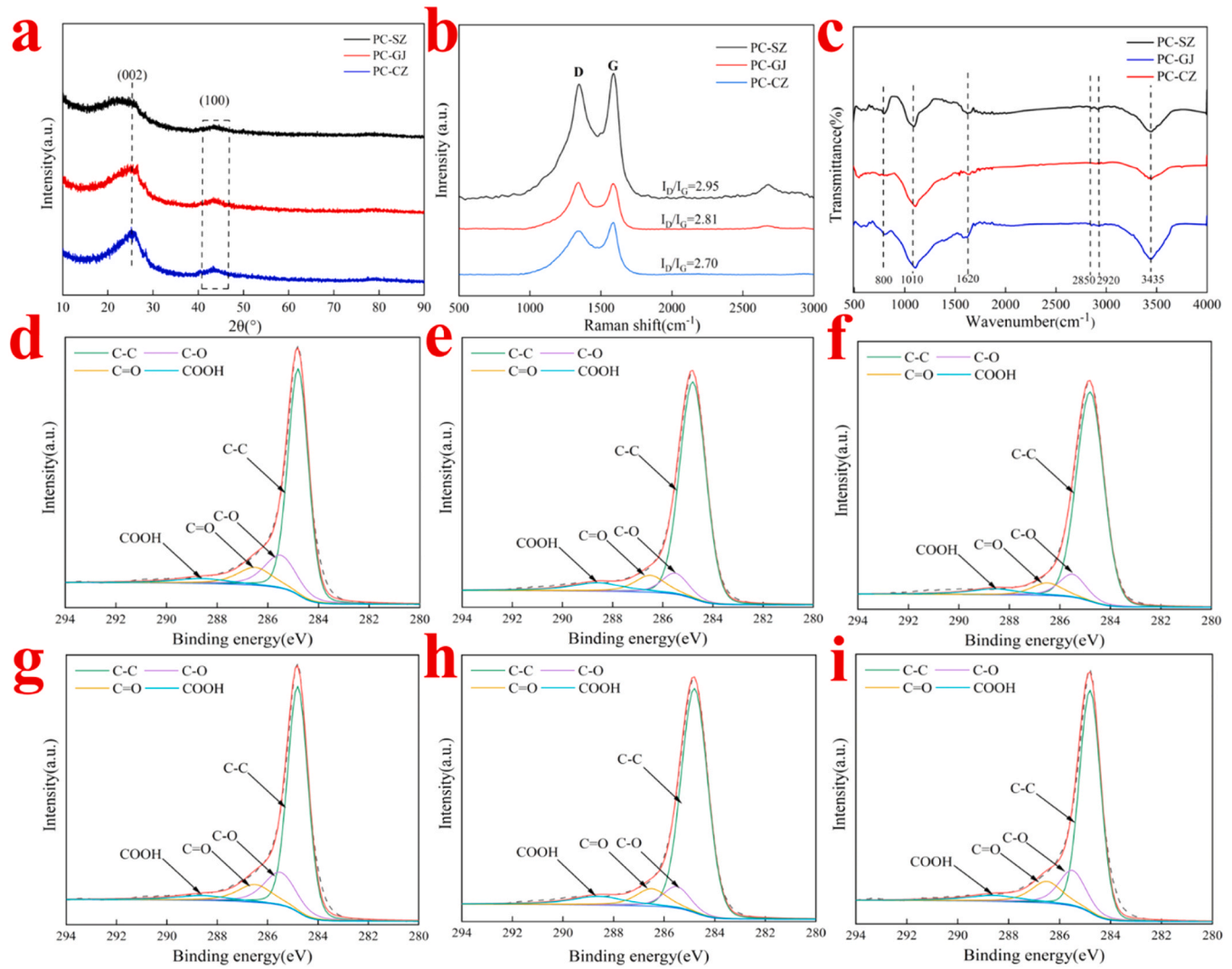

Fig. 6. (a) XRD spectra, (b) Raman spectra and (c) FTIR spectrogram of three Flash coal-based porous carbon; High resolution C ls spectrum of SZ (d), GJ (e), CZ (f), PC-SZ (d), PC-GJ (e) and PC-CZ (f).

stacked and the layer spacing gradually decreased. Raman spectroscopy is the most commonly used method for detecting defect structures in carbon materials. As shown in Fig. 6(b), two obvious peaks were found in the Raman spectrum located near 1350 and 1580 cm^{-1}. They were D peak and G peak respectively. D peak represented the content of defects in porous carbon, while the G peak represented the degree of order. The ratio of integrated area of D peak to G peak (ID/IG) is regarded as an indicator of defect density in porous carbon. The larger ratio indicated the higher defect degree. The ID/IG value of PC-SZ was the highest, followed by PC-GJ and PC-CZ, which proved that PC-SZ had maximum defect density.

Semiquantitative analysis was conducted on the surface functional groups and elemental content of Flash coal-based porous carbon through FTIR and XPS analysis. From Fig. 6(c), it can be seen that peaks around 3435 and 1100 cm^{-1} were corresponding to the stretching vibrations of hydroxyl and phenolic/alcoholic hydroxyl groups, respectively. The peak was noticed for the C═O stretching vibration about 1620 cm^{-1}. The peaks at 2850 and 2920 cm^{-1} may be for stretching vibration of $-CH_3$ and $-CH_2$. The peak at 798 cm^{-1} was caused by C-H bending vibration. The XPS C 1 s peaks fitting results of three coal and Flash coal-based porous carbon were demonstrated in Fig. 6(d-i). The content of elements and oxygen-containing functional groups were analyzed, and the results were shown in Table 5. The element C content in raw coal was higher than that in porous carbon, while the oxygen content was exactly the opposite. The oxidation reaction during the FJH process increases the oxygen content of porous carbon. PC-CZ had the lowest content of oxygen-containing functional groups (27.07%), while that in PC-SZ (31.59%) and PC-GJ (31.53%) was relatively low. The C-O and C═O content decreased from 28.18% to 23.07% as the degree of metamorphism of the raw coal increased. The rich pore structure and oxygen-containing functional groups content of porous carbon enable it to be used as an excellent adsorption material.

3.4. Adsorption of MB on Flash coal-based porous carbon

The adsorption performance of three Flash coal-based porous carbon was investigated by adsorbing MB and the adsorption kinetics was calculated. The curves of the adsorption quantity of MB on PC-SZ, PC-GJ and PC-CZ verse time were shown in Fig. 7. The amount of MB that adsorbed on porous carbon increased with time and reaching equilibrium after 80 min. It can be clearly seen that equilibrium adsorption capacity of PC-CZ was the highest, reaching 292 $mg{\cdot}g^{-1}$, that of PC-GJ and PC-CZ were 185 and 133 $mg{\cdot}g^{-1}$, respectively. The results showed that the adsorption capacity of PC-SZ on MB was superior to PC-GJ and PC-CZ. This might be due to the larger specific surface area that provided more adsorption sites on the PC-SZ surface.

The adsorption process could be fitted by the pseudo-first-order, pseudo-second-order and Weber-Morris intra-particle diffusion models to confirm the possible adsorption mechanism of MB on porous carbon surface. The confidence of fit was evaluated according to actual data based on the R^2 value (R^2 value was close or equal to 1 representing better fitting effect). Lagergren proposed the pseudo-first-order kinetic

Table 5
Element and oxygen-containing functional groups content of coal and Flash coal-based porous carbon.

Sample	Element and oxygen-containing functional group content measured from XPS (%)					Element O measured from organic element analyzer (%)
	C-C/ C═C	C-O	C═O	COOH	Element C (%)	
SZ	71.26	8.6	11.04	9.1	85.33	8.76
GJ	73.15	8.72	9.45	8.68	87.66	5.23
CZ	75.36	8.42	8.36	7.85	88.90	3.45
PC-SZ	68.41	17.38	10.8	3.41	87.25	11.57
PC-GJ	68.47	15.67	9.53	6.32	90.04	9.03
PC-CZ	72.93	15.59	7.48	4.00	90.29	8.21

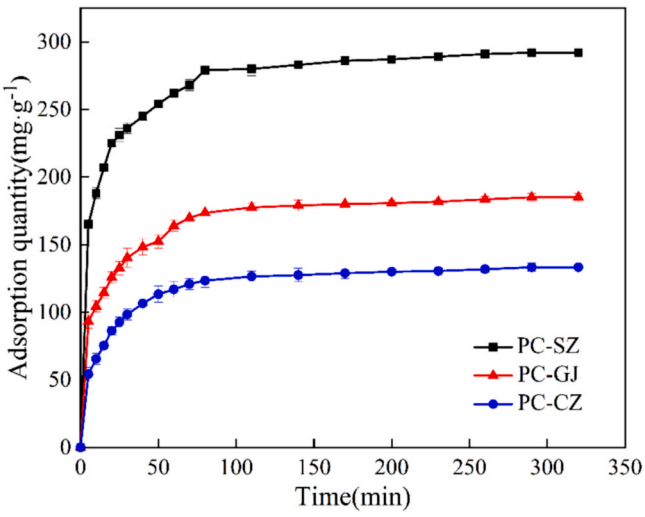

Fig. 7. Adsorption kinetics of MB on PC-SZ, PC-GJ and PC-CZ.

model, which assumes that adsorption is controlled by diffusion processes and the reaction rate is proportional to the amount of remaining adsorbate in the solution [40]. The integral equation of linear form is shown in Eq. (3).

$$\ln(Q_e - Q_t) = \ln Q_e - k_1 t \tag{3}$$

Where t is reaction time, min; Q_e and Q_t represent the adsorption quantity of MB on porous carbon at equilibrium and time t, $mg{\cdot}g^{-1}$; k_1 represents the pseudo-first-order rate constant, min^{-1}.

Listed in Table 6 showed the calculated kinetics parameters according to the experimental results. The fitting results were displayed in Fig. 8(a). It showed that R^2 value calculated was around 0.97, proving that the fitting effect was not very good. There is a significant difference between the experimental and calculated values of q_e. The pseudo-first-order model cannot explain the adsorption process commendably, indicating that MB adsorbed on Flash coal-based porous carbon was not primarily controlled by diffusion process.

According to the pseudo-second-order model, the adsorption process is mainly controlled by the chemical adsorption steps. The adsorption reaction rate constant of the adsorbate on the adsorbent is proportional to the square of the adsorbate concentration [41]. The linear expression after integration is shown in Eq. (4).

$$\frac{t}{Q_t} = \frac{1}{k_2 Q_e^2} + \frac{t}{Q_e} \tag{4}$$

Where k_2 is the pseudo-second-order reaction rate constant, $mg{\cdot}g^{-1}{\cdot}min^{-1}$. Table 6 showed the fitting values of coefficients and the fitting results were shown in Fig. 8(b). The R^2 values of the pseudo-second-order model were all greater than 0.99, and the value of q_e(cal.) was agreement with q_e(exp.). It implied that the pseudo-second-order model could effectively explain the adsorption process of MB on PC.

The Weber-Morris intra-particle diffusion model shown in Eq. (5) commonly considered that the adsorption process is divided into external mass transfer and intraparticle diffusion steps [42], intragranular adsorption is supposed to the ultimate stage of the entire adsorption process.

$$Q_t = k_{pi} t^{1/2} + C \tag{5}$$

Where k_{pi} is the intraparticle diffusion rate constant, $mg{\cdot}g^{-1}{\cdot}min^{-1/2}$; C is the constants related to boundary layer thickness, $mg{\cdot}g^{-1}$. The parameters were provided in Table 7. The fitting curves were shown in Fig. 8(c). As exhibited in Fig. 8(c), the adsorption process was divided

Table 6
Kinetic parameters of the pseudo-first-order and pseudo-second-order models.

Adsorbent	Q_e (cal.) (mg·g^{-1})	Pseudo-First-Order Model			Pseudo-Second-Order Model		
		k_1 (min^{-1})	Q_e (exp.) (mg·g^{-1})	R^2	k_2 (mg·g^{-1}·min^{-1})	Q_e (exp.) (mg·g^{-1})	R^2
PC-SZ	292.17	1.65×10^{-2}	92.98	0.98	3.40×10^{-3}	298.51	0.99
PC-GJ	185.00	1.51×10^{-2}	67.53	0.97	5.31×10^{-3}	190.11	0.99
PC-CZ	120.33	1.44×10^{-2}	52.44	0.97	8.02×10^{-3}	125.00	0.99

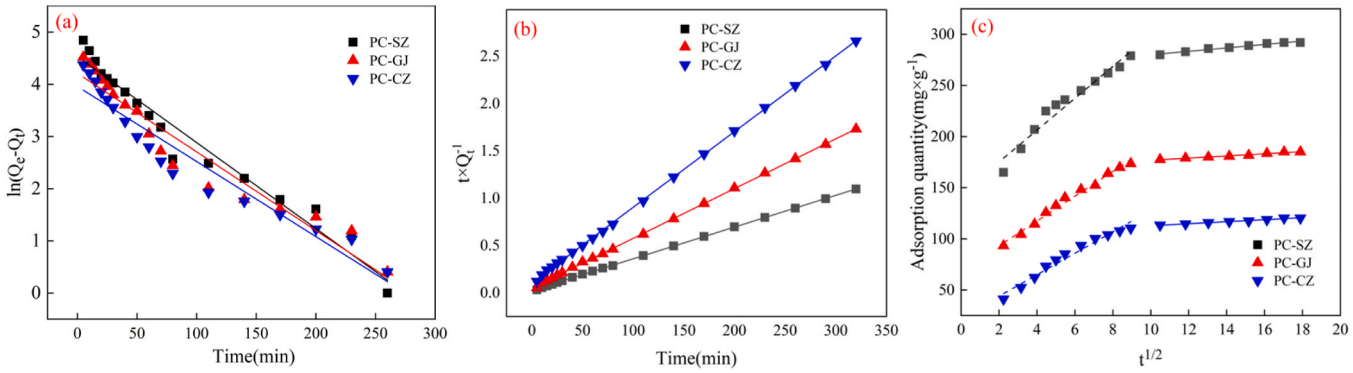

Fig. 8. Fitting results of: (a) pseudo-first-order model; (b) pseudo-second-order model;(c) Weber-Morris intra-particle diffusion model.

Table 7
Kinetic parameters of Weber-Morris intra-particle diffusion model.

Adsorbent	Stage	k_{pi} (mg·g^{-1}·min$^{-1/2}$)	C	R^2
PC-SZ	1st	1.68	263.27	0.99
	2nd	15.57	144.02	0.98
PC-GJ	1st	1.06	166.19	0.99
	2nd	12.13	68.89	0.99
PC-CZ	1st	0.98	102.94	0.99
	2nd	10.48	22.97	0.98

into two linear intervals, verifying the two adsorption stages. The significantly high linear slope of the first interval indicated that MB can rapidly diffuse to the outer surface of porous carbon. The lower linear slope of the second interval was because of the low adsorption rate from the outer surface diffusion of porous carbon to the inner pores.

The results showed that the adsorption of MB on porous carbon could be legitimately described by pseudo-second-order kinetic model. Chemical adsorption dominated the entire adsorption process. It is undoubtfully that the diffusion process also affected the adsorption process. The difference in adsorption performance of three Flash coal-based porous carbon might be due to the differences in physical and chemical properties. Therefore, it is necessary to understand the physical and chemical properties of three coal-based porous carbon to determine the underlying adsorption mechanism.

Fig. 9 showed the adsorption mechanism of MB on PC-SZ, PC-GJ and PC-CZ. The specific surface area of porous carbon was the initial factor affecting adsorption performance. In general, porous carbon with a large specific surface area has more pores, especially micropores and mesopores, providing more adsorption sites for adsorbates, resulting in better adsorption performance. PC-SZ had the largest specific surface area and well-developed micropores, which was beneficial for the adsorption of MB on its surface. People believed that the molecular diameter of MB was approximately 1.2 nm with a line-shaped structure [43]. The most ideal adsorbent pore size is just slightly larger than the adsorbed molecules. The number of pores within the range of 1.2–5 nm in PC-SZ was greater than that in PC-GJ, followed by PC-CZ. Therefore, the difference in the number of micropores and mesopores was the main reason for the difference of three porous carbons. As a result, PC-SZ had the best adsorption effect on MB. Besides, the chemical structure of porous carbon can also affect its adsorption performance. The interlayer spacing of PC-SZ was the largest and there were many defects, which was beneficial for MB molecules to enter and adsorb on porous carbon surfaces. That in PC-GJ and PC-CZ was relatively low, the adsorption performance was poor. Meanwhile, the amount of oxygen-containing functional groups in porous carbon played a significant role in the adsorption of MB. The surface of PC-SZ and PC-GJ carbon contained many negatively charged oxygen-containing functional groups, which were easy to absorb positively charged MB under the action of electrostatic attraction [44]. Therefore, the adsorption performance of PC-CZ for MB was weaker

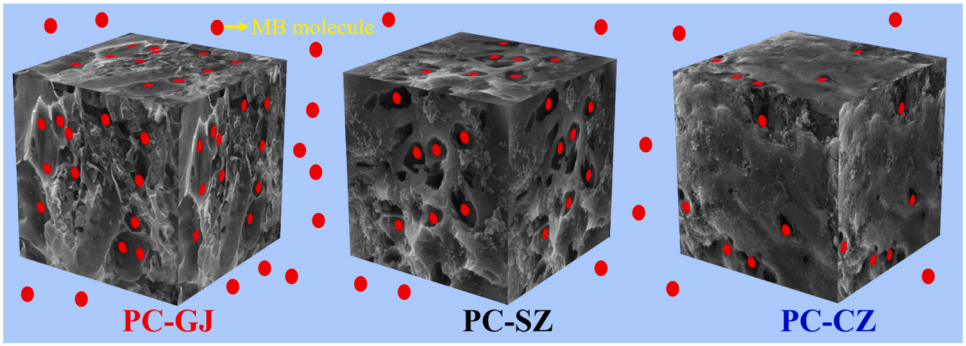

Fig. 9. Adsorption mechanism of MB on PC-SZ, PC-GJ and PC-CZ.

than that of PC-SZ and PC-GJ.

4. Conclusion

Flash Joule heating method eliminated the need for prolonged heating and highly polluting chemical treatment, achieving the rapid preparation of porous carbon with excellent adsorption performance. The degree of metamorphism of bituminous coal led to differences in physical and chemical properties of the prepared porous carbon. The higher volatile content of low metamorphic bituminous coal was conducive to the pore development of porous carbon, and the prepared porous carbon had a specific surface area of 601.95 $m^2 \cdot g^{-1}$. Porous carbon prepared from low metamorphic degree bituminous coal possessed more lattice defects and oxygen-containing functional groups and a lower degree of graphitization. The maximum adsorption capacity of Flash Porous carbon for MB reached 292.17 $mg \cdot g^{-1}$. The diffusion process and chemical adsorption dominated the adsorption process. PC-SZ with more micropore and defects would provide more chemical adsorption sites for MB. Meanwhile, the negatively charged oxygen-containing functional groups on the surface of porous carbon were easily adsorbed with positively charged MB under electrostatic interaction. The results proved that FJH method achieved the preparation of porous carbon with excellent adsorption performance. This method provides a new approach for the green and efficient preparation of porous carbon, which is expected to achieve large-scale production.

CRediT authorship contribution statement

Qiang Li: Investigation, Methodology, Writing – original draft, Writing – review & editing. **Yajun Wang:** Methodology, Formal analysis, Software. **Rongtao Zhu:** Conceptualization, Resources, Supervision, Writing – review & editing. **Junchen Wu:** Methodology, Resources, Software. **Wenjun Zhang:** Investigation, Methodology, Supervision, Writing – review & editing. **Haozhi Lu:** Methodology, Software.

Declaration of Competing Interest

The authors declare that they have no known competing financial interests or personal relationships that could have appeared to influence the work reported in this paper.

Data availability

Data will be made available on request.

Acknowledgments

This research was funded by the National Natural Science Foundation of China (Grant No. 51974307), Key Research and Development Project of Xuzhou City (KC21287), the Graduate Innovation Program of China University of Mining and Technology (2023WLKXJ064), the Postgraduate Research & Practice Innovation Program of Jiangsu Province (KYCX23_2814), and supported by the Fundamental Research Funds for the Central Universities (No. 2023XSCX019).

References

[1] H. Li, X. He, T. Wu, B. Jin, L. Yang, J. Qiu, Synthesis, modification strategies and applications of coal-based carbon materials, Fuel Process. Technol. 230 (2022), 107203, https://doi.org/10.1016/j.fuproc.2022.107203.
[2] Y. Qiao, R. Zhang, R. Li, W. Fang, Z. Cui, D. Zhang, Green preparation of hierarchical porous carbon with tunable pore size for supercapacitors, Ionics 27 (2021) 3077–3087, https://doi.org/10.1007/s11581-021-04091-0.
[3] Y. Zhu, Y. Wang, T. Wang, H. Liu, H. Liu, M. Zang, One-step preparation of coal-based magnetic activated carbon with hierarchically porous structure and easy magnetic separation capability for adsorption applications, J. Magn. Magn. Mater. 569 (2023), 170480, https://doi.org/10.1016/j.jmmm.2023.170480.
[4] X.M. Yue, Z.Y. An, M. Ye, Z.J. Liu, C.C. Xiao, Y. Huang, Y.J. Han, S.Q. Zhang, J. S. Zhu, Preparation of porous activated carbons for high performance supercapacitors from taixi anthracite by multi-stage activation, Molecules 24 (2019) 3588, https://doi.org/10.3390/molecules24193588.
[5] G. Gong, S. Liang, Y. Shi, Z. Wang, Z. Li, R. Li, S. Lu, Y. Zhang, Preparation of microporous carbon materials using residual coal from oxidative degradation of lignite as the carbon source and the mechanism and dynamics of its methyl orange adsorption, Colloids Surf. A Physicochem. Eng. Asp. 636 (2022), 128138, https://doi.org/10.1016/j.colsurfa.2021.128138.
[6] C. Chen, Q. Fu, X. Chen, G. He, J. Ye, C. Zhou, K. Hu, L. Cheng, M. Zhao, An effective pre-burning treatment boosting adsorption capacity of sorghum distillers' grain derived porous carbon, Diam. Relat. Mater. 124 (2022), 108914, https://doi.org/10.1016/j.diamond.2022.108914.
[7] M. Yang, C. Fang, H. Zeng, J. Su, Y. Cheng, L. Pei, M. Liu, Porous carbon derived from waste corrugated paper board using different activators, J. Mater. Cycles Waste Manag. 24 (2022) 1893–1901, https://doi.org/10.1007/s10163-022-01446-1.
[8] X. Zhang, X. Ma, Z. Yu, Y. Yi, Z. Huang, C. Lu, Preparation of high-value porous carbon by microwave treatment of chili straw pyrolysis residue, Bioresour. Technol. 360 (2022), 127520, https://doi.org/10.1016/j.biortech.2022.127520.
[9] Y. Liu, H. Cui, J. Xu, J. Shi, N. Yan, J. Zou, S. You, Direct synthesis of honeycomb-like porous carbons from potassium cinnamate for CO_2 capture, Mater. Lett. 344 (2023), 134443, https://doi.org/10.1016/j.matlet.2023.134443.
[10] H. Tian, J. Pan, D. Zhu, Z. Guo, C. Yang, Y. Xue, S. Li, Y. Wang, Innovative one-step preparation of activated carbon from low-rank coals activated with oxidized pellets, J. Clean. Prod. 313 (2021), 127877, https://doi.org/10.1016/j.jclepro.2021.127877.
[11] Y. Chen, Z. He, S. Ding, M. Wang, H. Liu, M. Hou, X. Chen, J. Gao, L. Wang, C. P. Wong, Facilely preparing lignin-derived graphene-ferroferric oxide nanocomposites by flash Joule heating method, Res. Chem. Intermed. 49 (2023) 589–601, https://doi.org/10.1007/s11164-022-04883-7.
[12] W.A. Algozeeb, P.E. Savas, D.X. Luong, W. Chen, C. Kittrell, M. Bhat, R. Shahsavari, J.M. Tour, Flash graphene from plastic waste, ACS Nano 14 (2020) 15595–15604, https://doi.org/10.1021/acsnano.0c06328.
[13] P.A. Advincula, D.X. Luong, W. Chen, S. Raghuraman, R. Shahsavari, J.M. Tour, Flash graphene from rubber waste, Carbon 178 (2021) 649–656, https://doi.org/10.1016/j.carbon.2021.03.020.
[14] Z. Sun, Y.H. Hu, Ultrafast, low-cost, and mass production of high-quality graphene, Angew. Chem. Int. Ed. 59 (2020) 9232–9234, https://doi.org/10.1002/anie.202002256.
[15] O. Vieira, R.S. Ribeiro, J.L. Diaz de Tuesta, H.T. Gomes, A.M.T. Silva, A systematic literature review on the conversion of plastic wastes into valuable 2D graphene-based materials, Chem. Eng. J. 428 (2022), 131399, https://doi.org/10.1016/j.cej.2021.131399.
[16] K.M. Wyss, D.X. Luong, J.M. Tour, Large-scale syntheses of 2D materials: flash joule heating and other methods, Adv. Mater. 34 (2022) 1–27, https://doi.org/10.1002/adma.202106970.
[17] D. Dong, Y. Zhang, Y. Xiao, T. Wang, J. Wang, W. Gao, Oxygen-enriched coal-based porous carbon under plasma-assisted MgCO3 activation as supercapacitor electrodes, Fuel 309 (2022), 122168, https://doi.org/10.1016/j.fuel.2021.122168.
[18] J. Wang, Y. Cui, Y. Gu, H. Xu, Y. Shi, Z. Ju, Q. Zhuang, Coal-based modified carbon for high performance sodium-ion battery, Solid State Ion. 368 (2021), 115701, https://doi.org/10.1016/j.ssi.2021.115701.
[19] Y. Yang, X. Yang, Q. Jia, S. Zheng, Z. Lin, Z. Qin, Enhanced photocatalytic performance of (N, F) co-doped TiO2 loaded on coal-based hierarchical porous carbon foam under simulated sunlight, Vacuum 207 (2023), 111577, https://doi.org/10.1016/j.vacuum.2022.111577.
[20] L. Wang, F. Sun, J. Gao, X. Pi, Z. Qu, G. Zhao, Adjusting the porosity of coal-based activated carbons based on a catalytic physical activation process for gas and liquid adsorption, Energy Fuels 32 (2018) 1255–1264, https://doi.org/10.1021/acs.energyfuels.7b03211.
[21] S. Yonghui, L. Siming, Y. Ning, H. Wenjin, Treatment of cyanide wastewater dynamic cycle test by three-dimensional electrode system and the reaction process analysis, Environ. Technol. 42 (2021) 1693–1702, https://doi.org/10.1080/09593330.2019.1677783.
[22] P. Vassileva, A. Detcheva, Removal of toxic ions from aqueous solutions using lignite-coal-based activated carbons modified by oxidation, Int. J. Coal Prep. Util. 31 (2011) 242–257, https://doi.org/10.1080/19392699.2011.558547.
[23] Z. Yi, J. Yao, M. Zhu, H. Chen, F. Wang, X. Liu, Kinetics, equilibrium, and thermodynamics investigation on the adsorption of lead(II) by coal-based activated carbon, Springerplus 5 (2016), 1160, https://doi.org/10.1186/s40064-016-2839-4.
[24] P. Huang, R. Zhu, X. Zhang, W. Zhang, A milliseconds flash joule heating method for the regeneration of spent cathode carbon, J. Environ. Sci. Health Part A Toxic/Hazard. Subst. Environ. Eng. 57 (2022) 33–44, https://doi.org/10.1080/10934529.2021.2022422.
[25] P. Ostaszewski, O. Długosz, M. Banach, Analysis of measuring methods of the concentration of methylene blue in the sorption process in fixed-bed column, Int. J. Environ. Sci. Technol. 19 (2022) 1–8, https://doi.org/10.1007/s13762-021-03156-x.
[26] J. Tang, L. Feng, Y. Li, J. Liu, X. Liu, Fractal and pore structure analysis of Shengli lignite during drying process, Powder Technol. 303 (2016) 251–259, https://doi.org/10.1016/j.powtec.2016.09.042.
[27] J.Z. Liu, J.F. Zhu, J. Cheng, J.H. Zhou, K.F. Cen, Pore structure and fractal analysis of Ximeng lignite under microwave irradiation, Fuel 146 (2015) 41–50, https://doi.org/10.1016/j.fuel.2015.01.019.

[28] J. Hoslett, H. Ghazal, N. Mohamad, H. Jouhara, Removal of methylene blue from aqueous solutions by biochar prepared from the pyrolysis of mixed municipal discarded material, Sci. Total Environ. 714 (2020), 136832, https://doi.org/10.1016/j.scitotenv.2020.136832.
[29] J. Georgin, D.S.P. Franco, M.S. Netto, D. Allasia, M.L.S. Oliveira, G.L. Dotto, Treatment of water containing methylene by biosorption using Brazilian berry seeds (Eugenia uniflora), Environ. Sci. Pollut. Res. 27 (2020) 20831–20843, https://doi.org/10.1007/s11356-020-08496-8.
[30] W. Chen, J. Chen, K.V. Bets, R.V. Salvatierra, K.M. Wyss, G. Gao, C.H. Choi, B. Deng, X. Wang, J.T. Li, C. Kittrell, N. La, L. Eddy, P. Scotland, Y. Cheng, S. Xu, B. Li, M.B. Tomson, Y. Han, B.I. Yakobson, J.M. Tour, Battery Metal Recycling by Flash Joule Heating, 2023, pp. 1–14. https://doi.org/10.1126/sciadv.adh5131.
[31] W. Chen, R.V. Salvatierra, J.T. Li, C. Kittrell, J.L. Beckham, K.M. Wyss, N. La, P. E. Savas, C. Ge, P.A. Advincula, P. Scotland, L. Eddy, B. Deng, Z. Yuan, J.M. Tour, Flash recycling of graphite anodes, Adv. Mater. 35 (2023) 1–14, https://doi.org/10.1002/adma.202207303.
[32] Y. Yao, K.K. Fu, S. Zhu, J. Dai, Y. Wang, G. Pastel, Y. Chen, T. Li, C. Wang, T. Li, L. Hu, Carbon welding by ultrafast joule heating, Nano Lett. 16 (2016) 7282–7289, https://doi.org/10.1021/acs.nanolett.6b03888.
[33] L. Li, X. Wang, S. Wang, Z. Cao, Z. Wu, H. Wang, Y. Gao, J. Liu, Activated carbon prepared from lignite as supercapacitor electrode materials, Electroanalysis 28 (2016) 243–248, https://doi.org/10.1002/elan.201500532.
[34] Q.P. Campbell, J.R. Bunt, H. Kasaini, D.J. Kruger, The preparation of activated carbon from South African coal, J. S. Afr. Inst. Min. Metall. 112 (2012) 37–44.
[35] H. Zhao, L. Wang, D. Jia, W. Xia, J. Li, Z. Guo, Coal based activated carbon nanofibers prepared by electrospinning, J. Mater. Chem. A. 2 (2014) 9338–9344, https://doi.org/10.1039/c4ta00069b.
[36] Y. Zou, H. Wang, L. Xu, M. Dong, B. Shen, X. Wang, J. Yang, Synergistic effect of CO_2 and H2O co-activation of Zhundong coal at a low burn-off rate on high performance supercapacitor, J. Power Sources 556 (2023), 232509, https://doi.org/10.1016/j.jpowsour.2022.232509.
[37] Z. Chen, A. Zhang, C. Geng, J. Xiong, P. Sun, N. Tu, Y. Chen, J. Jiang, Z. Ju, Coal-based hierarchical porous carbon for lithium/potassium storage, Mater. Chem. Phys. 303 (2023) 1–9, https://doi.org/10.1016/j.matchemphys.2023.127835.
[38] S. Wang, J. Wang, Synthesis and electrochemical performance of porous carbon derived from medium and low temperature coal pitch, Int. J. Electrochem. Sci. 17 (2022), 221281, https://doi.org/10.20964/2022.12.88.
[39] Y. Önal, C. Akmil-Başar, Ç. Sarici-Özdemir, Investigation kinetics mechanisms of adsorption malachite green onto activated carbon, J. Hazard. Mater. 146 (2007) 194–203, https://doi.org/10.1016/j.jhazmat.2006.12.006.
[40] P. Kowalczyk, A.P. Terzyk, G. Piotr A, G. Rychlicki, Numerical analysis of the Horvath-Kawazoe equation - the adsorption of nitrogen, argon, benzene, carbon tetrachloride and sulphur hexafluoride, Adsorpt. Sci. Technol. 20 (2002) 295–306, https://doi.org/10.1260/026361702760254478.
[41] W. Plazinski, W. Rudzinski, A. Plazinska, Theoretical models of sorption kinetics including a surface reaction mechanism: a review, Adv. Colloid Interface Sci. 152 (2009) 2–13, https://doi.org/10.1016/j.cis.2009.07.009.
[42] A. Aurich, J. Hofmann, R. Oltrogge, M. Wecks, R. Gläser, L. Blömer, S. Mauersberger, R.A. Müller, D. Sicker, A. Giannis, Improved isolation of microbiologically produced (2R,3S)-isocitric acid by adsorption on activated carbon and recovery with methanol, Org. Process Res. Dev. 21 (2017) 866–870, https://doi.org/10.1021/acs.oprd.7b00090.
[43] D. Li, J. Li, Q. Gu, S. Song, C. Peng, Co-influence of the pore size of adsorbents and the structure of adsorbates on adsorption of dyes, Desalin. Water Treat. 57 (2016) 14686–14695, https://doi.org/10.1080/19443994.2015.1065446.
[44] P. Van Hao, P.N. Minh, P.N. Hong, N.N. Huy, P.T. Oanh, H.T. Nguyen, T.D. Tran, D. Van Thanh, V.T.K. Nguyen, N. Van Dang, Gram-scale synthesis of electrochemically oxygenated graphene nanosheets for removal of methylene blue from aqueous solution, Nanotechnology 32 (2021) 16LT01, https://doi.org/10.1088/1361-6528/abdc8b.